Chapter 21

Condensation in Microchannels

Summary: A state-of-the-art of condensation heat transfer small channels (microchannels and minichannels) is described here. This chapter addresses experimental studies and prediction methods for condensation inside of such small channels, together with some comparisons of these methods to selected experimental data sets and to one another. Also, a brief overview of numerical simulation of annular laminar condensing flows is included. For the benefit of the reader who has a special interest in this topic, Chapter 20 presents a detailed overview of microscale two-phase flow fundamentals and flow pattern maps (as well as boiling heat transfer); thus, Chapter 20 contains many details relevant to condensation in microchannels: macro-to-microscale transition criteria, flow pattern maps, void fractions, pressure drops, etc.

21.1 Introduction

In general, macroscale intube condensation methods are not reliable when extrapolated down to much smaller channel sizes, in particular below about 3 mm in diameter. Naturally, if one takes experimental results for condensation in say a 1 mm channel and makes a comparison to one of the dozens of macroscale condensation correlations, it is probable that one will work. But, realistically, this is likely just a coincidence because then taking the same method and comparing it to data at other diameters or other fluids, one finds that the fit is no longer satisfactory. There is, however, no proven guideline to use to differentiate between macroscale condensation and microscale condensation, and hence no proven rule for when to use a microscale method instead of a macroscale method. Some preliminary methods for the macroscale-to-microscale transition have been presented in Chapter 20 that can be used as an approximate guideline. Furthermore, it is even more inappropriate to extrapolate flow pattern based condensation methods developed for macroscale to microscale channels since the underlying flow pattern map typically does not extrapolate very well either.

The change in the controlling phenomena and heat transfer mechanisms when passing from macrochannel condensation heat transfer to microchannels is not as evident as the transition in flow boiling discussed in Chapter 20. Perhaps the most important effect is from the surface tension (capillary) forces because most microchannel geometries used for condensation, such as those in extruded aluminum multi-port tubes, are not circular; hence the capillary forces tend to draw the condensate to the corners and this augments heat transfer on the remaining perimeter. Thus, it is important to remember that the circular microchannel methods presented in this chapter are not generally reliable when extrapolating them to non-circular channels using a hydraulic diameter, an approach which totally ignores the capillary effect. Furthermore, quite often microscale condensation data fall into the *laminar* slug and *laminar* annular flow regimes and therefore new dimensionless groups may come into play as the dominant factors while the influence of others may disappear. Hence, even though it can be done using a significantly large number of empirical constants, it is usually not theoretically logical to empirically refit macroscale methods to microscale data since a different combination of non-dimensional numbers is then controlling. On the other hand, if one is considering turbulent annular film condensation in a microchannel, the difference between that and the same process in a macrochannel would appear to not be so different. Hence, one must always keep in mind the flow pattern and physical aspects of the flow on heat transfer when addressing both macroscale and microscale condensation.

21.1.1 Objectives of this chapter

A concise summary of research on condensation in microchannels is presented here. It is not the objective here to describe *all* the work that has been published on this topic, but instead to present a compact treatment of some typical experimental results, describe some prediction methods developed specifically for microscale channels and propose an assessment of where we stand today on the most important topics. This chapter addresses microchannel condensation topics in the following order: (*i*) an overview of the experimental microscale condensation studies, (*ii*) a presentation of the empirical methods proposed specifically for microscale condensation heat transfer, (*iii*) some comparison of these competing methods, and (*iv*) a brief treatment of the status of numerical modeling of microscale condensation.

Notably, the interested reader is also referred to the chapter by Garimella in the book of Kandlikar, Garimella, Li, Colin and King (2005) for an extensive review of macroscale and microscale condensation. Other condensation reviews and papers are also worthy to note, such as those by Webb and Zhang (1998), Cavallini et al. (2006), Kandlikar (2007) and Chen et al. (2008). For an extensive study on flow patterns during condensation in small channels, both circular and non-circular, refer to Coleman and Garimella (2003).

21.1.2 Applications of microscale condensation

Numerous applications for microscale condensation are in use or are emerging. The most important so far is their use in compact condensers for automotive air-conditioning systems with multi-port aluminum tubes, which have internal diameters on the order of 0.7 to 1.5 mm. All of these applications require thermal design methods that are accurate, reliable and robust (that is, methods that follow the trends of the data well and work for a multitude of fluids, channel sizes and shapes, pressures, flow rates, heat fluxes, etc.). Presently, the state-of-the-art is only partially able to fulfill such requirements as these channels often have non-circular cross-sectional shapes for which no method has been of proven general validity so far.

For the design and fabrication of ultra-compact plate condensers using microscale convective condensation for transferring heat, Wolverine Tube Inc. has developed a new patented technique called **Micro Deformation Technology** (MDT). Figure 21.1 shows an example of such fin geometries. The process can produce fin densities up to as high as about 1000 fins per inch (fpi) or 40 fins per mm or more, interfin spacings for channels as small as about 0.0004 in. (0.010 mm) with fins up to as high as about 0.03 in. (0.76 mm), depending on the material (copper, copper alloys, aluminum, low carbon and stainless steels, titanium, plastic, PTFE, etc.). Wetted surface area ratios relative to the base area can be as high as 14 times and perhaps more depending on the material. The fins can be made into closed multi-microchannel cooling elements by adding an enclosure. Thus, it is possible to make these finned surfaces into ultra-compact evaporators, condensers, single-phase heat exchangers, etc. For more information on these surfaces and their applications, refer to the Wolverine Tube Inc. website: http://www.wlv.com.

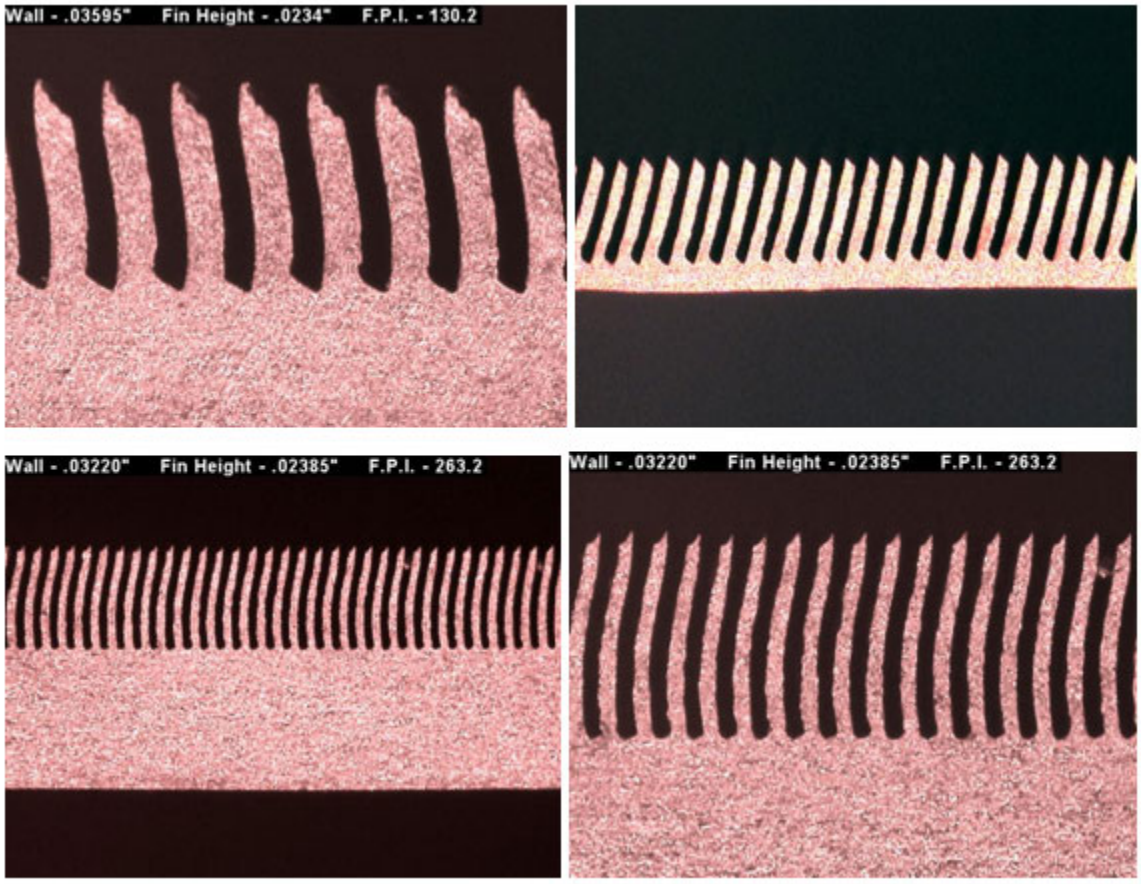

Figure 21.1. Photographs of ultra high density finned surfaces manufactured with Wolverine Tube Inc. Micro Deformation Technology (MDF). Upper left: 130 fpi (5.1 fin/mm) surface; upper right: 185 fpi (7.3 fins/mm) surface with fin height of 0.022 in. (0.56 mm) and fin thickness one-half of fin pitch; lower left and right: 263.2 fpi (10.4 fins/mm) surface.

21.2 Experimental Microscale Condensation Studies

Some experimental studies are on single channels while others are on multi-port flat extruded aluminum tubes with multiple channels in parallel. Experiments on non-circular cross-sectional channels are primarily for rectangular or square channels, but other geometries that have been tested include triangular, trapezoidal, etc. Some examples of the types of geometries tested by Garimella and coworkers are shown in Figure 21.2. Figure 21.3 shows photographs of the multi-port tubes tested by Koyama et al. (2003a, 2003b).

Tables 21.1 and 21.2 summarize many (but not all) of the numerous experimental studies in channels less than 3 mm in diameter with circular and noncircular cross-sections, respectively. Quite a few experimental studies have been done on condensation in small diameter channels. Table 21.3 summarizes the experimental studies on microchannels with diameters less than 300 μm. Most of these microchannels were fabricated in a silicon wafer and hence have non-circular cross sections, such as rectangular or trapezoidal shapes, due to the etching process. Detailed information of the operating range and test section configuration is summarized in these tables. Notably, nearly all the data are for a horizontal channel orientation.

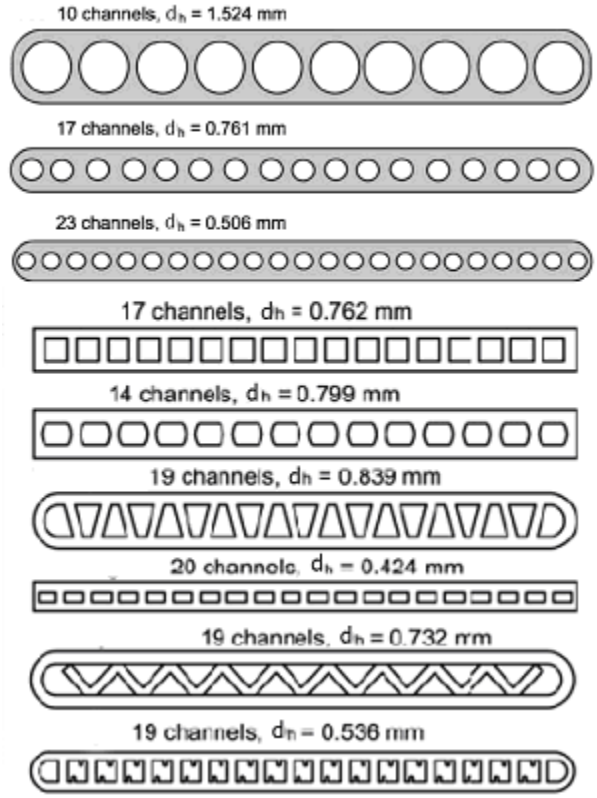

Figure 21.2. Circular and non-circular tubes shapes and hydraulic diameters tested by Bandhauer, Agarwal and Garimella (2006) and Agarwal, Bandhauer and Garimella (2007).

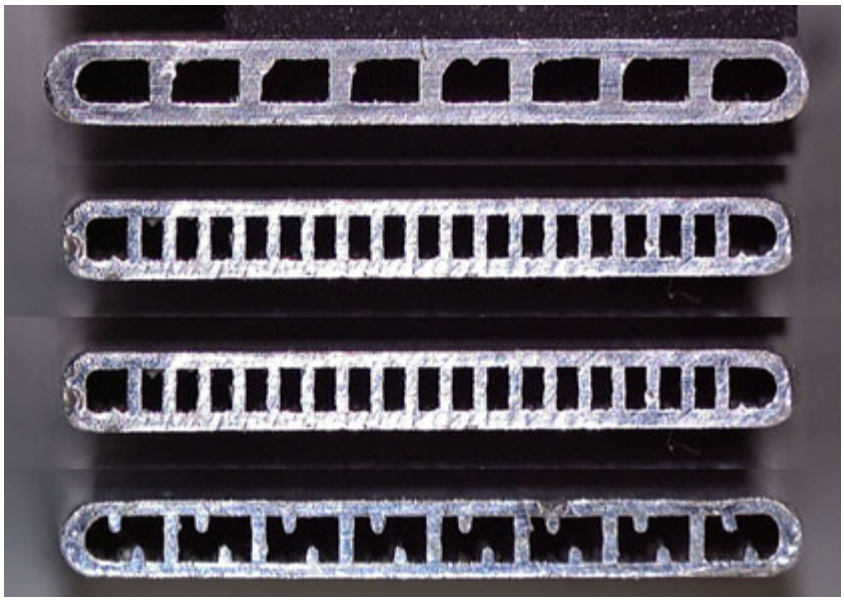

Figure 21.3. Multi-port extruded aluminum flat tubes tested by Koyama et al. (2003a, 2003b).

Table 21.1. Condensation heat transfer studies in small circular channels.

Reference	Fluid	Diameter [mm]	Single or multi-channel	Shape	Orientation	T_{sat} [°C] or p_{sat}	$\dot{m}$ [kg/m^{2}s]	q [kW/m^2]	x
Dobson and Chato (1998)	R22, R134a, R32/R125	3.14-7.04	Single	Circular	Horizontal	35-45	75-800	5-15	0.1-0.9
Yan and Lin (1999)	R134a	2	Multi	Circular	Horizontal	25-50	100-200	10-20	0-1
Wang and Du (2000)	Water	1.94-4.98	Single	Circular	Inclined	1-1.5 MPa	11-95	-	0-1
Coleman and Garimella (2003)	R134a	2.67-4.91	Multi	Circular	Horizontal		150-750	-	-
Begg, Holley and Faghri (2003)	Water	1.7-4	Single	Circular	Horizontal	60-90	10-25	-	-
Baird, Fletcher and Haynes (2003)	R123, R11	0.92, 1.95	Single	Circular	Horizontal	20-72	70-600	15-110	0-1
Shin and Kim (2004)	R134a	0.691	Single	Circular	Horizontal	40	100-600	5-20	0.1-0.9
Shin and Kim (2005)	R134a	0.494-1.067	Single	Circular	Horizontal	40	100-600	5-20	0.15-0.85
Bandhauer, Agarwal and Garimella (2006)	R134a	0.506-1.524	Multi	Circular	Horizontal	50-60	150-750	-	0-1
Matkovic et al. (2009)	R134a, R32	0.96	Single	Circular	Horizontal	40	100-1200	-	0.03-0.99

Table 21.2. Condensation heat transfer studies in small non-circular channels.

Reference	Fluid	Hydraulic Diameter [mm]	Single or multi-channel	Shape	Orientation	T_{sat} [°C] or p_{sat}	$\dot{m}$ [kg/m^{2}s]	q [kW/m^2]	x
Yang and Webb (1996)	R12	2.637	Multi	Rect-angular	Horizontal	65	400-1400	4-12	0.1-1
Chang, Tsai and Hwang (1997)	R134a, R22	0.72-1.13	Multi	Rect-angular	Horizontal	1-2.1 MPa	30-100	-	0.5-1
Webb and Ermis (2001)	R134a	0.44-1.564	Multi	Rect-angular	Horizontal	65	300-1000	8	0.1-0.9
Wang, Radcliff and Christensen (2002)	R134a	1.46	Multi	Rect-angular	Horizontal	61-66.5	75-750	-	0.03-0.94
Coleman and Garimella (2003)	R134a	2.67-4.91	Multi	Rect-angular	Horizontal		150-750	-	-
Kim et al. (2003)	R22, R410	1.41	Multi	Rect-angular	Horizontal	45	200-600	5-15	0.1-0.9
Koyama et al. (2003a), Koyama et al. (2003b)	R134a	0.807-1.062	Multi	Rect-angular	Horizontal	60	100-700	-	0-1
Wilson et al. (2003)	R134a, R410	1.84-7.79	Single	Flattened	Horizontal	35	75-400	-	0.1-0.8
Cavallini et al. (2005)	R134a, R410a	1.4	Multi	Rect-angular	Horizontal	40	200-1400	-	0.25-0.75
Shin and Kim (2005)	R134a	0.494-1.067	Single	Rect-angular	Horizontal	40	100-600	5-20	0.15-0.85
Agarwal, Bandhauer and Garimella (2007)	R134a	0.424-0.839	Multi	Non-circular	Horizontal	50-60	150-750	-	0-1
Fernando et al. (2008)	Propane	1.42	Multi	Rect-angular	Vertical	30-50	20-50	4-10	-

Table 21.3. Condensation heat transfer studies in very small channels (less than 0.3 mm in diameter).

Reference	Fluid	Hydraulic Diameter [mm]	Single or multi-channel	Shape	Orientation	T_{sat} [°C] or p_{sat}	$\dot{m}$ [kg/m^{2}s]	q [kW/m^2]	x
Chen and Cheng (2005)	Water	0.075	Multi	Trapezoidal	Horizontal	0.13-0.23 MPa	-	-	-
Wu and Cheng (2005), Cheng and Wu (2005)	Water	0.083	Multi	Trapezoidal	Horizontal	0.13-0.42 MPa	193-475	-	-
Agarwal and Garimella (2007)	R134a	0.1-0.2	Multi	Rectangular	Horizontal	30-60	200-800	-	1-0
Hu and Chao (2007)	Water	0.07-0.24	Multi	Trapezoidal	Horizontal	-	5-45	6-40	-
Dong and Yang (2008)	R141b	0.067-0.117	Multi	Rectangular	Horizontal	-	50-500	-	-
Quan, Chen and Wu (2008)	Water	0.11-0.26	Multi	Trapezoidal	Horizontal	-	100-250	-	0.1-0.8
Wu et al. (2008)	Water	0.075-0.129	Multi	Trapezoidal	Horizontal	-	-	-	-
Zhang, Xu and Thome (2008)	Water	0.058	Single	Rectangular	Horizontal	0.12-0.21 MPa	173-630	-	-
Zhang, Xu and Liu (2008)	Water	0.058	Multi	Rectangular	Horizontal	0.12-0.21 MPa	109-229	-	-

Accurate measurement of the local heat transfer coefficient is quite a challenge in microchannels because water cooling is required, as opposed to applying an electrical heat flux in boiling experiments. Therefore, a small temperature rise in the coolant results in a large uncertainty in the estimation of the heat flux. Furthermore, in condensation it is difficult to measure local heat transfer coefficients and hence mostly quasi-local values are measured, i.e. mean values for a change in the vapor quality over a length of the test section. To improve the accuracy of heat transfer measurements, different measurement techniques have been developed. For instance, a novel technique was developed by the Garimella's group that uses a secondary loop to amplify the coolant's temperature rise (the primary coolant) by using a secondary coolant with a lower flow rate. This significantly increased the accuracy of the heat flux estimation, see for instance Bandhauer, Agarwal and Garimella (2006) and Agarwal, Bandhauer and Garimella (2007). Another novel technique for the heat flux measurement was developed by Shin and Kim (2004, 2005);

they cooled an electric-heating mockup in parallel to their condensing unit and adjusted the heating input in the mockup to match the same surface temperature with the actual test section. Furthermore, Koyama et al. (2003a, 2003b) employed thermo-electric sensors to measure the local heat flux. In summary, careful analysis of the experimental uncertainties and selection of the most appropriate measurement technique are necessary to build an accurate test facility for condensation research in small diameter channels. Importantly, it is also imperative to pre-validate such test setups with subcooled liquid tests to determine their heat losses to the environment and to compare their single-phase turbulent heat transfer coefficients against commonly used heat transfer correlations.

Figure 21.4 illustrates some microchannel experimental data taken by the Matkovic et al. (2009) for R-134a condensing inside a horizontal 0.96 mm circular channel at a nominal saturation temperature of 40°C. The tests were made using a novel water cooling flow on the outside of the channel to insure good mixing of the water along the test section. The mass velocities illustrated range from 100 to 1200 kg/m^{2}s. As can be noted, the mass velocity has only a minor effect at the lower end of the mass velocity range, especially at the lowest vapor qualities, but a major effect overall. Furthermore, the heat transfer coefficients decrease with decreasing vapor quality and the slope of the data decreases as the mass velocity decreases. These trends are in fact similar to those also found in macrochannel condensation studies and other microchannel studies.

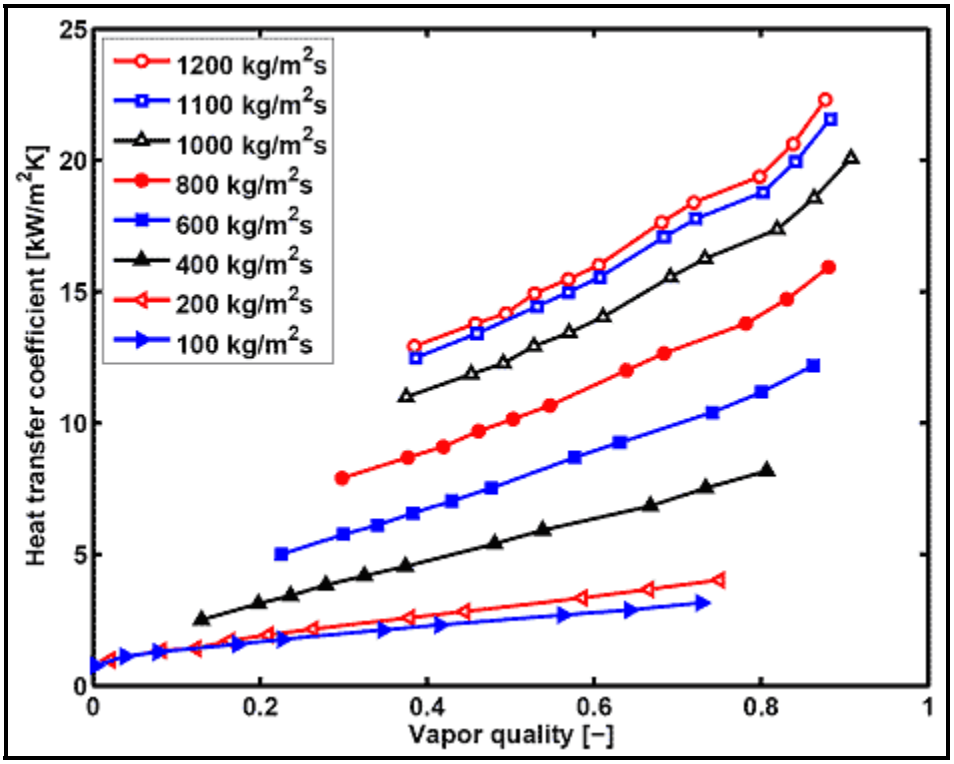

Figure 21.4. Experimental data of Matkovic et al. (2009) for R-134a in a single 0.96 mm channel at 40°C saturation temperature and mass velocities from 100 to 1200 kg/m^{2}s.

Figure 21.5 depicts some more heat transfer coefficients from Agarwal, Bandhauer and Garimella (2007) for condensing R-134a at a nominal refrigerant saturation temperature of 55°C in a square multi-channel test section with hydraulic channel diameters of 0.762 mm. The trends are similar to those in the above study.

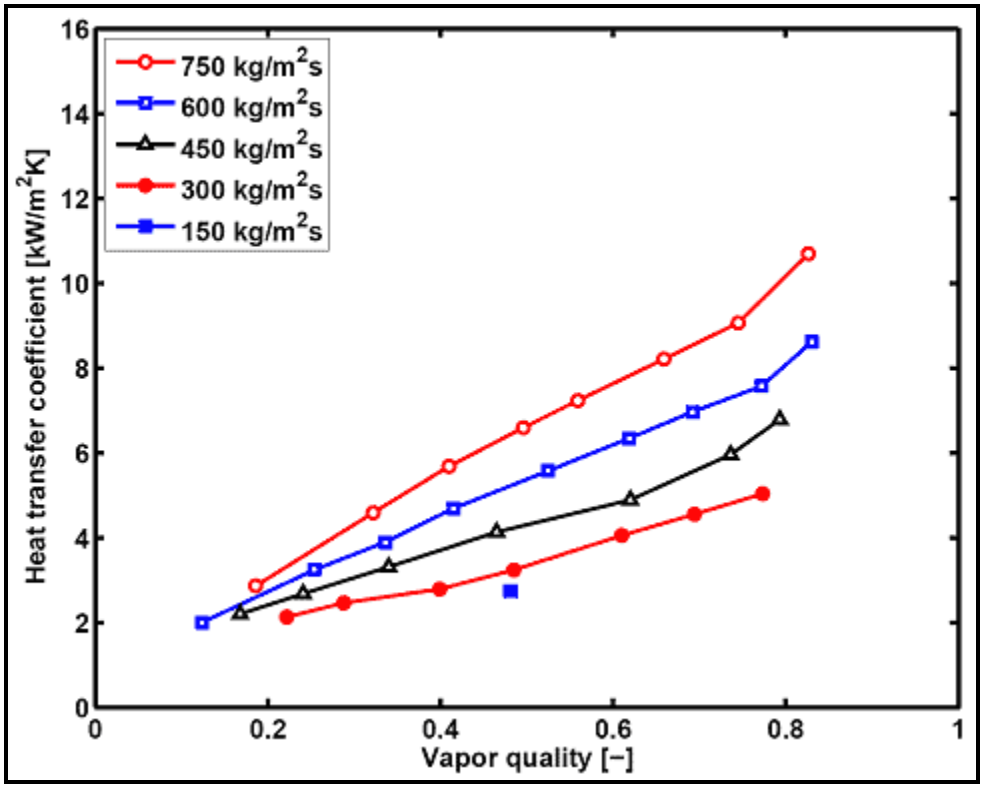

Figure 21.5. Heat transfer coefficients for condensing R-134a at a nominal refrigerant saturation temperature of 55°C in square multi-channels with hydraulic diameters of 0.762 mm from Agarwal, Bandhauer and Garimella (2007).

21.3 Microscale Condensation Prediction Methods

The most widely used macroscale methods for channel diameters from about 3 mm and up are presented in Chapter 8 and are not repeated here. It is common to find some of these macroscale methods compared to microchannel condensation data, even though the macroscale correlations are usually developed only from turbulent two-phase flow data while microscale data may also fall into the laminar slug and laminar annular flow regimes, rendering such comparisons somewhat illogical. Nevertheless, for small databases for a particular fluid and microchannel diameter, it is not surprising if one of the numerous macroscale methods happens by chance to fit the data. One should not, however, then mistakenly conclude that such a method will work for other microchannel data.

Furthermore, most methods developed for condensation in microchannels are empirical variations on prior macroscale methods. Hence, even though this can be done, sometimes by adding a significant number of new empirical constants, it is not necessarily theoretically logical to do this since a different combination of non-dimensional numbers is probably controlling the heat transfer process. On the other hand, if one is considering turbulent annular film condensation in a microchannel, the difference between that and the same process in a macrochannel would appear to not be so different. The biggest differences may come from the much smaller thicknesses in the annular film, the relative entrainment of droplets into the core flow of vapor, the size of interfacial waves, capillary effects on non-circular channels, etc. Furthermore, flow pattern transitions are effected by the small channels (also the absence of stratified

flow regimes in microchannels) and hence flow pattern based methods will normally not scale down well from macroscale and microscale channels.

Presently, not all of the numerous microchannel condensation predicting methods that are available in the literature will be presented here. Instead, the five methods that appear to be most appropriate for small channels were selected and are described below. The complete details of each formulation can be found in the original publication.

Moser, Webb and Na method. The Moser, Webb and Na (1998) method is one of the widely cited models developed by the research group of Webb. This model was developed using a large database from 18 sources for channel diameters from 3.14 mm to 20 mm; hence, it is strictly a macroscale method but it has been found to work reasonably well for microchannels. This method uses an equivalent Reynolds number method based on the heat-momentum analogy, which states that a relationship exists between heat transfer and the wall stress. By assuming liquid-only artificial conditions resulting in the same interfacial shear stress, they defined an equivalent Reynolds number. Their formulation for the local Nusselt number for the local condensing heat transfer coefficient α(x) is expressed using the equivalent Reynolds number as follows:

$$\mathrm{Nu}(x) = \frac{\alpha(x) d_i}{k_L} = \frac{0.0994^{a}\ \mathrm{Re}_L^{b}\ \mathrm{Re}_{eq}^{1+0.875a}\ \mathrm{Pr}_L^{0.815}}{(1.58 \ln \mathrm{Re}_{eq} - 3.28)(2.58 \ln \mathrm{Re}_{eq} + 13.7\, \mathrm{Pr}_L^{2/3} - 19.1)} \qquad [21.3.1]$$

The empirical exponents in this expression are calculated in terms of the liquid Prandtl number Pr_L as:

$$a = 0.126\, \mathrm{Pr}_L^{-0.448} \qquad [21.3.2a]$$

$$b = -0.113\, \mathrm{Pr}_L^{-0.563} \qquad [21.3.2b]$$

The liquid Prandtl number is defined as:

$$\mathrm{Pr}_L = \frac{\mu_L c_{pL}}{k_L} \qquad [21.3.3]$$

The equivalent liquid Reynolds Re_{eq} is formulated with a two-phase multiplier on the liquid Reynolds number Re_{Lt} for all the flow as liquid:

$$\mathrm{Re}_{eq} = \left(\Phi_{fr}^2\right)^{8/7} \mathrm{Re}_{Lt} \qquad [21.3.4]$$

$$\mathrm{Re}_{Lt} = \frac{\dot{m}_{total}\, d_i}{\mu_L} \qquad [21.3.5]$$

The empirical two-phase multiplier was taken from the Friedel (1979) frictional two-phase pressure drop correlation (see Chapter 13), whose two-phase multiplier is:

$$\Phi_{fr}^2 = E + \frac{3.24\, F\, H}{\mathrm{Fr}_H^{0.045}\ \mathrm{We}_L^{0.035}} \qquad [21.3.6]$$

The dimensionless factors Fr_H, E, F and H are as follows:

$$Fr_H = \frac{\dot{m}_{total}^2}{g d_i \rho_H^2} \quad [21.3.7]$$

$$E = (1-x)^2 + x^2 \frac{\rho_L f_G}{\rho_G f_L} \quad [21.3.8]$$

$$F = x^{0.78}(1-x)^{0.224} \quad [21.3.9]$$

$$H = \left(\frac{\rho_L}{\rho_G}\right)^{0.91} \left(\frac{\mu_G}{\mu_L}\right)^{0.19} \left(1 - \frac{\mu_G}{\mu_L}\right)^{0.7} \quad [21.3.10]$$

The liquid Weber We_L is defined as:

$$We_L = \frac{\dot{m}_{total}^2 d_i}{\sigma \rho_H} \quad [21.3.11]$$

The following definition of the homogeneous density ρ_H based on vapor quality is used:

$$\rho_H = \left(\frac{x}{\rho_G} + \frac{1-x}{\rho_L}\right)^{-1} \quad [21.3.12]$$

The friction factors are calculated by the Blasius friction factor correlation for turbulent flow (see Chapter 13).

Koyama and coworkers method. Koyama et al. (2003a) evaluated their previous macroscale condensation model, proposed in Haraguchi, Koyama and Fujii (1994), with their new experimental data for microchannels. They found that the pressure drop correlation employed in their macroscale condensation model was unable to predict the forced convective pressure drop well in their microchannel tests. Therefore, by employing the microscale method of Mishima and Hibiki (1995) for the frictional pressure drop instead, they obtained better heat transfer predictions, indicating that shear stress plays an important role in determining the heat transfer coefficient. In their new method, the condensation heat transfer is expressed as an asymptotic combination of the forced convection condensation and gravity controlled condensation terms:

$$Nu = \frac{\alpha(x) d_i}{k_L} = (Nu_c^2 + Nu_{grav}^2)^{1/2} \quad [21.3.13]$$

The forced convection condensation term is given by the empirical relationship:

$$Nu_c = 0.0152(1 + 0.6\,Pr_L^{0.8}) \left(\frac{\Phi_G}{X_{tt}}\right) Re_L^{0.77} \quad [21.3.14]$$

The two phase multiplier factor from the Mishima and Hibiki correlation is:

$$\Phi_G^2 = 1 + 21(1 - e^{-0.319 d_i})X_{tt} + X_{tt}^2 \quad [21.3.15]$$

The Lockhart-Martinelli parameter and liquid fraction Reynolds number are:

$$X_{tt} = \left(\frac{1-x}{x}\right)^{0.9}\left(\frac{\rho_V}{\rho_L}\right)^{0.5}\left(\frac{\mu_L}{\mu_V}\right)^{0.1} \quad [21.3.16]$$

$$Re_L = \frac{\dot{m}_{total}(1-x)d_i}{\mu_L} \quad [21.3.17]$$

On the other hand, the gravity controlled convection condensation is calculated using the void fraction ε, the Galileo number Ga_L and the Jacob number Ja_L as follows:

$$Nu_{grav} = 0.725\,H(\varepsilon)\left(\frac{Ga_L\,Pr_L}{Ja_L}\right)^{1/4} \quad [21.3.18]$$

$$H(\varepsilon) = \varepsilon + \{10(1-\varepsilon)^{0.1} - 1 + 1.7\times10^{-4}\,Re_L\}\sqrt{\varepsilon}(1-\sqrt{\varepsilon}) \quad [2.13.19]$$

$$Ga_L = \frac{g\rho_L^2 d_i^3}{\mu_L^2} \quad [21.3.20]$$

$$Ja_L = \frac{c_{pL}(T_{sat} - T_{wall})}{h_{LG}} \quad [21.3.21]$$

The void fraction is calculated using the momentum flux expression of Smith (1969) assuming a fixed value of entrainment e = 0.4 (see Chapter 17):

$$\varepsilon = \left[1 + \frac{\rho_V}{\rho_L}\left(\frac{1-x}{x}\right)\left(0.4 + 0.6\sqrt{\frac{\frac{\rho_V}{\rho_L} + 0.4\frac{1-x}{x}}{1 + 0.4\frac{1-x}{x}}}\right)\right]^{-1} \quad [21.3.22]$$

Curiously, the gravity controlled process is based on the void fraction but the void fraction is not used to model the liquid velocity or liquid film thickness in the convective heat transfer coefficient expression.

Cavallini and coworkers method. Cavallini et al. (2006) proposed a condensation heat transfer method considering liquid entrainment, developed from a large database from different laboratories covering a wide range of channel diameters (mostly macroscale data). This method was recently found to accurately predict the Matkovic et al. (2009) condensation data for a 0.96 mm circular microchannel in tests with R134a and R32. In their method, the local condensation heat transfer coefficient is a function of the shear stress and dimensionless temperature:

$$\alpha(x) = \rho_L c_{pL}(\tau_i/\rho_L)^{0.5}/T^+ \quad [21.3.23]$$

The dimensionless temperature T^+ is calculated using the dimensionless film thickness δ^+ and liquid fraction Reynolds number (with an entrained liquid correction) using the following equations:

$$T^+ = \delta^+ \, Pr_L \qquad \delta^+ \le 5 \qquad [21.3.24]$$

$$T^+ = 5\left\{Pr_L + \ln\left[1 + Pr_L(\delta^+/5 - 1)\right]\right\} \qquad 5 < \delta^+ < 30 \qquad [21.3.25]$$

$$T^+ = 5\left\{Pr_L + \ln(1 + 5\,Pr_L) + 0.495\ln(\delta^+/30)\right\} \qquad \delta^+ \ge 30 \qquad [21.3.26]$$

$$\delta^+ = (Re_L/2)^{0.5} \text{ for } Re_L \le 1145 \qquad [21.3.27]$$

$$\delta^+ = 0.0504\,Re_L^{7/8} \text{ for } Re_L > 1145 \qquad [21.3.28]$$

$$Re_L = \dot{m}_{total}(1-x)(1-e)d_i/\mu_L \qquad [21.3.29]$$

In the last expression above, e is the entrainment rate, i.e. the fraction of the liquid flowing in the vapor phase. The shear stress is determined with the following equations:

$$\tau_i = (dp/dz)_{frict}\, d_i/4 \qquad [21.3.30]$$

$$(dp/dz)_{frict} = \Phi_L^2 (dp/dz)_{frict,L} = \Phi_L^2\, 2 f_L \dot{m}_{total}^2/(d_i \rho_L) \qquad [21.3.31]$$

$$\Phi_L^2 = Z + 3.595\,F\,H\,(1-e)^W \qquad [21.3.32]$$

$$W = 1.398 p_r \qquad [21.3.33]$$

$$Z = (1-x)^2 + x^2(\rho_L/\rho_G)(\mu_L/\mu_G)^{0.2} \qquad [21.3.34]$$

$$F = x^{0.9525}(1-x)^{0.414} \qquad [21.3.35]$$

$$H = (\rho_L/\rho_G)^{1.132}(\mu_G/\mu_L)^{0.44}(1-\mu_G/\mu_L)^{3.542} \qquad [21.3.36]$$

$$f_L = 0.046(\dot{m}_{total}\, d_i/\mu_L)^{-0.2} \text{ for any } Re_L \qquad [21.3.37]$$

Here, p_r is the reduced pressure. The entrainment rate is given by Paleev and Filippovich correlation [3].

$$e = 0.015 + 0.44\log\left[(\rho_{Gc}/\rho_L)(\mu_L U_G/\sigma)^2 10^4\right] \qquad [21.3.38]$$

This expression is valid for e < 0.95 but when e is calculated to be larger than 0.95, e is set equal to 0.95. Other parameters are the density of the gas core and vapor superficial velocity:

$$\rho_{Gc} = \rho_G(1 + (1-x)e/x) \qquad [21.3.39]$$

$$U_G = \frac{\dot{m}_{total}\, x}{\rho_G} \qquad [21.3.40]$$

Garimella and coworkers methods. The Bandhauer, Agarwal and Garimella (2006) and Agarwal, Bandhauer and Garimella (2007) methods were developed by the research group lead by Garimella for circular microchannels and non-circular microchannels, respectively. The method for circular minichannels is as follows:

$$\alpha(x) = \frac{\rho_L c_{pL} u^*}{T^+} \qquad [21.3.41]$$

Here, the turbulent dimensionless temperature T^+ and the turbulent dimensionless radius of the channel R^+ are defined for a channel of radius R as:

$$T^+ = 5\left\{Pr_L + \ln\left[1 + Pr_L(\delta^+/5 - 1)\right]\right\} \text{ for } Re_L < 2100 \quad [21.3.42]$$

$$T^+ = 5\,Pr_L + 5\ln(5\,Pr_L + 1) + \int_{30}^{\delta^+} \frac{dy^+}{\left(\frac{1}{Pr_L} - 1\right) + \frac{y^+}{5}\left(1 - \frac{y^+}{R^+}\right)} \text{ for } Re_L \geq 2100 \quad [21.3.43]$$

$$R^+ = \frac{R\rho_L u^*}{\mu_L} \quad [21.3.44a]$$

$$y^+ = \frac{y\rho_L u^*}{\mu_L} \quad [21.3.44b]$$

Here, y is the length scale (used for film thickness). The dimensionless liquid film thickness is given by:

$$\delta^+ = \frac{\delta\rho_L u^*}{\mu_L} \quad [21.3.45]$$

$$\delta = (1 - \sqrt{\varepsilon})\frac{d_i}{2} \quad [21.3.46]$$

The friction velocity is defined as:

$$u^* = \sqrt{\frac{\tau_i}{\rho_L}} \quad [21.3.47]$$

The interfacial shear stress is determined from the pressure drop gradient:

$$\tau_i = \left(\frac{dp}{dz}\right)_{frict}\frac{d_i}{4} \quad [21.3.48]$$

The frictional pressure drop gradient is defined using an empirical method involving the void fraction:

$$\left(\frac{dp}{dz}\right)_{frict} = \frac{1}{2} f_i \frac{\dot{m}_{total}^2 x^2}{\rho_G \varepsilon^{2.5} d_i} \quad [21.3.49]$$

The void fraction is determined by:

$$\varepsilon = \left[1 + \left(\frac{1-x}{x}\right)^{0.74}\left(\frac{\rho_G}{\rho_L}\right)^{0.65}\left(\frac{\mu_L}{\mu_G}\right)^{0.13}\right]^{-1} \quad [21.3.50]$$

The interfacial friction factor is computed from:

$$f_i = f_L A x^a Re_L^b \psi^c \quad [21.3.51]$$

where

$$\mathrm{Re}_L = \frac{\dot{m}_{total}(1-x)d_i}{(1+\sqrt{\varepsilon})\mu_L} \quad [21.3.52]$$

$$\text{for } \mathrm{Re}_L < 2100: \ A = 0.001308, \quad a = 0.427, \quad b = 0.930, \quad c = -0.121 \quad [21.3.53]$$

$$\text{for } \mathrm{Re}_L > 3400: \ A = 25.64, \quad a = 0.532, \quad b = -0.327, \quad c = 0.021 \quad [21.3.54]$$

For the transition region data, the friction factor is first independently calculated using the high and low values of the mass velocity corresponding to the laminar and turbulent boundaries. A linear interpolation between these bounding values is then conducted to get the friction factor corresponding to the actual mass velocity. The same process is repeated with the vapor quality instead of the mass velocity. By averaging these two interpolated values, the interfacial friction factor in transition region can be estimated using

$$f_L = \frac{64}{\mathrm{Re}_L} \text{ for } \mathrm{Re}_L < 2100 \quad [21.3.55]$$

$$f_L = \frac{0.136}{\mathrm{Re}_L^{0.25}} \text{ for } \mathrm{Re}_L > 3400 \quad [21.3.56]$$

Here, the Martinelli parameter is given by:

$$X = \left[\frac{(dp/dz)_L}{(dp/dz)_G}\right]^{1/2} \quad [21.3.57]$$

where

$$\left(\frac{dp}{dz}\right)_L = \frac{1}{2} f_L \frac{\dot{m}_{total}^2 (1-x)^2}{\rho_L d_i} \quad [21.3.58]$$

$$\left(\frac{dp}{dz}\right)_G = \frac{1}{2} f_G \frac{\dot{m}_{total}^2 x^2}{\rho_G d_i} \quad [21.3.59]$$

$$\psi = \frac{U_L \mu_L}{\sigma} \quad [21.3.60]$$

$$U_L = \frac{\dot{m}_{total}(1-x)}{\rho_L (1-\varepsilon)} \quad [21.3.61]$$

Agarwal, Bandhauer and Garimella (2007) evaluated the Bandhauer, Agarwal and Garimella (2006) model versus their noncircular channel data and found that it failed to adequately predict their data. The mismatch was attributed to the pressure drop model. Therefore, they optimized the shear stress correlation with experimental data of each particular channel geometry, as reported in Agarwal and Garimella (2006). With the newly optimized parameter, the data for round edged non-circular channels were better predicted; however, since the model needed a different optimized expression for each geometry, this involves extrapolation when applying it to a new geometry. In addition, the data for the sharp edged non-circular channels were not predicted well with the annular flow assumption. Therefore, they proposed to

use a mist flow "homogeneous" model for the sharp edged configuration. The mist flow based correlation they proposed is:

$$Nu = \frac{\alpha(x) d_i}{k_G} = 0.00345\, Re_H^{0.9} \left(\frac{\mu_G h_{LG}}{k_G (T_{sat} - T_{wall})} \right)^{1/3} \quad [21.3.62]$$

The homogenous Reynolds number and homogeneous dynamic viscosity were determined as follows:

$$Re_H = \dot{m}_{total}\, d_i / \mu_H \quad [21.3.63]$$

$$\frac{1}{\mu_H} = \frac{x}{\mu_G} + \frac{(1-x)}{\mu_L} \quad [21.3.64]$$

They proposed to use the homogeneous flow type of model for sharp edged non-circular channels and annular flow model (using the non-circular pressure drop method) for round edged non-circular channels.

21.4 Comparison of Microscale Condensation Prediction Methods to Data

In this section, the results of an internal study by Park, Consolini and Thome (2009) are presented. In this study, the five methods described above were compared with a selection of independent experimental data (that is, data not used in the development of the particular method). The first comparison was to the data available for circular channels of Bandhauer, Agarwal and Garimella (2006) to three of the other methods. The tests were conducted with R134a in the multi-port tubes shown in Figure 21.2. As can be seen in Figure 21.6, the comparison of these three methods to independent data shows that two of them are able to capture about two-thirds of the data within ±20% with acceptable mean average errors of about 20% or less.

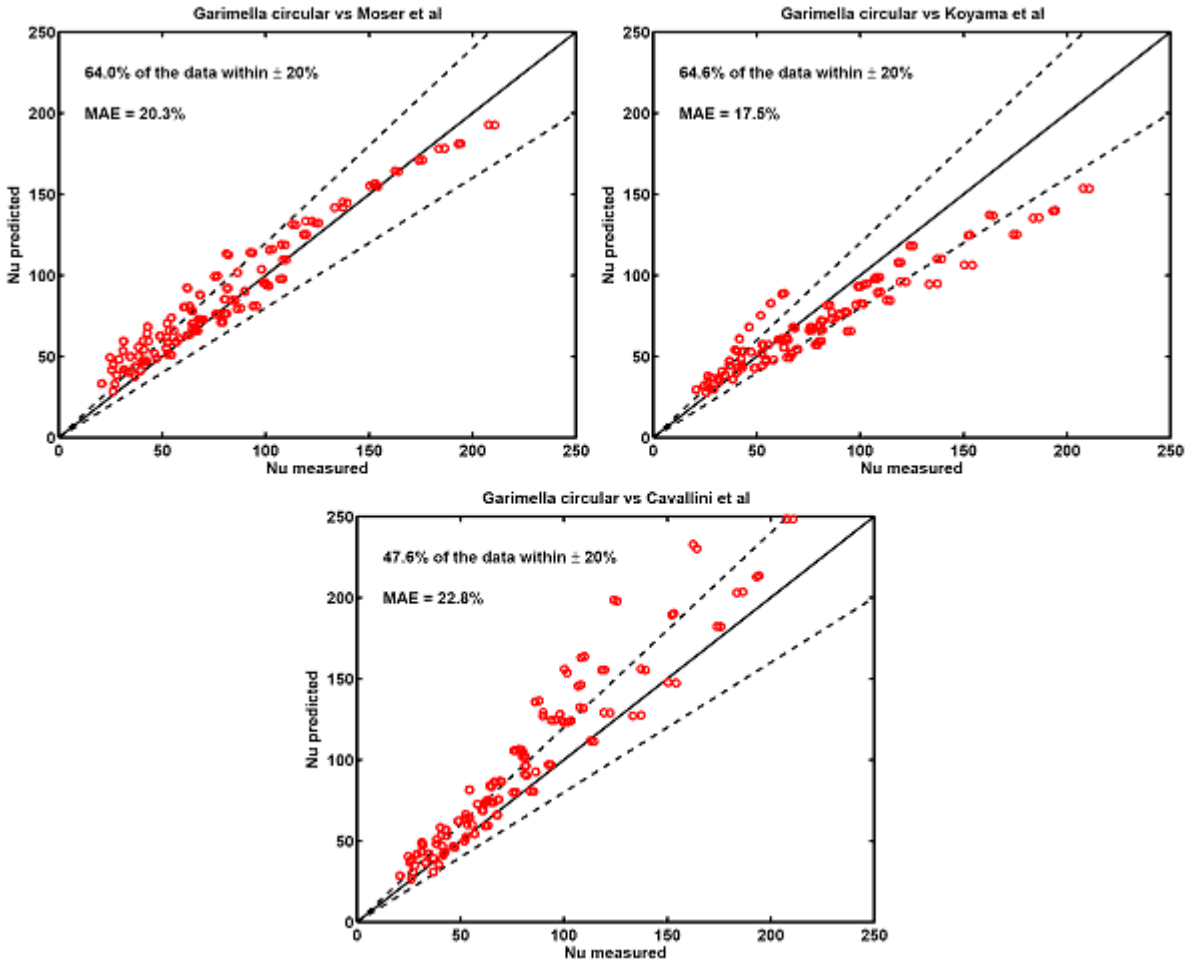

Figure 21.6. Predicted Nusselt numbers compared to the circular channel data of Bandhauer, Agarwal and Garimella (2006).

The second comparison is versus the independent circular microchannel data set of Shin and Kim (2004, 2005) in Figure 21.7. The method of Moser, Webb and Na (1998) again worked reasonably well while that of Bandhauer, Agarwal and Garimella (2006) gave very accurate predictions, capturing 84.1% of the data within ±20%.

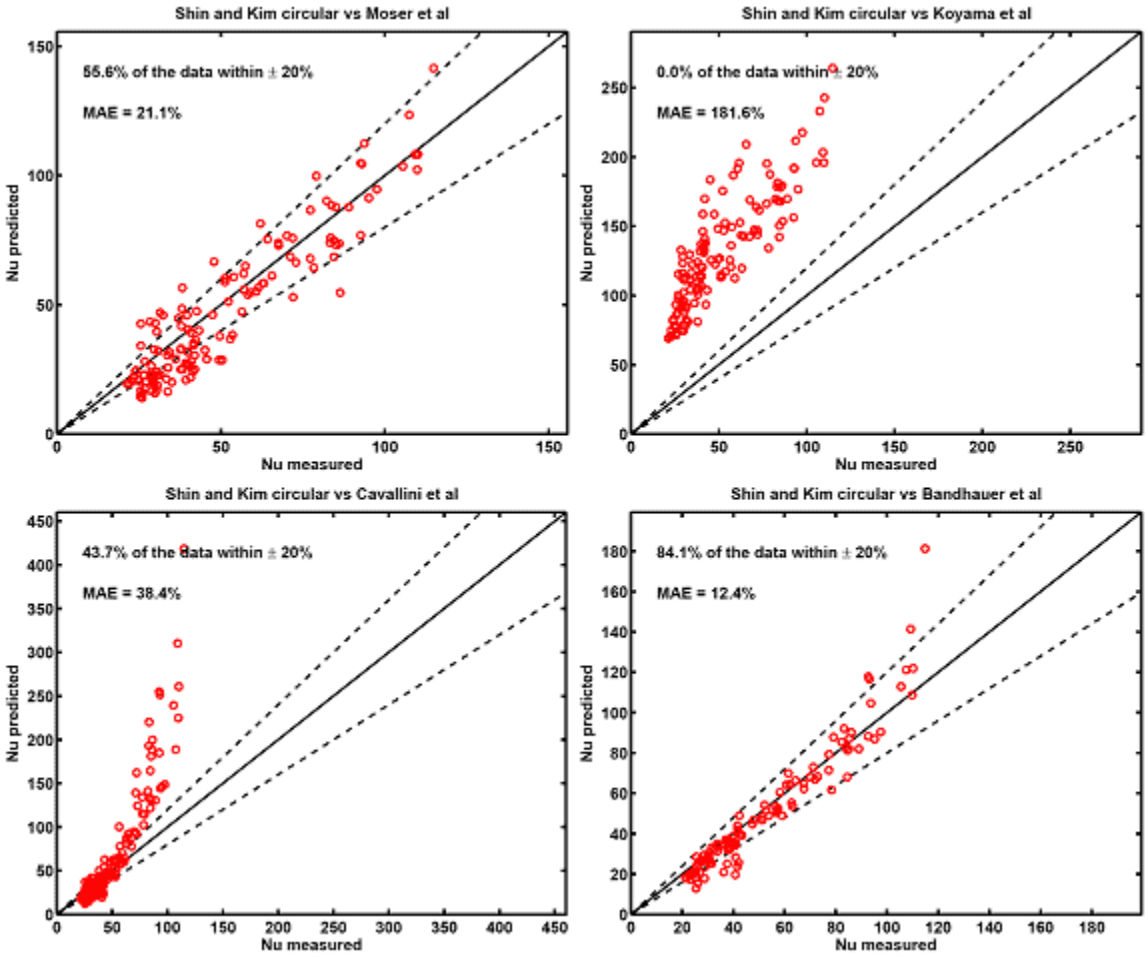

Figure 21.7. Predicted Nusselt numbers compared to the circular channel data from Shin and Kim (2004, 2005).

Figure 21.8 shows a comparison of three methods to the independent round edged non-circular channel data of Agarwal, Bandhauer and Garimella (2007). As can be seen, the best method in this case is that of Koyama et al. (2003a). Figure 21.9 depicts three methods compared to the independent non-circular channel with sharp edge data of Agarwal, Bandhauer and Garimella (2007). In this case, it is the Cavallini et al. (2006) to be the only acceptable method. Figure 21.10 finally shows a comparison of four methods versus the non-circular channel data from Shin and Kim (2004). Here, the Agarwal, Bandhauer and Garimella (2007) method was the only one to give acceptable predictions, followed by the method of Moser, Webb and Na (1998).

In summary, as can be discerned from the description of the methods, most of the prediction methods intimate that the frictional pressure gradient plays an important role in determining the heat transfer. Thus, in small diameter channels, the accurate prediction of the frictional pressure gradient becomes of paramount importance. Furthermore, the above evaluation found that condensation heat transfer data in small and microchannels similar behavior from that in macrochannels. Also notable, it seems that non-circular microchannel data have different trends than the circular microchannel data when the conventional hydraulic diameter definition is used to implement the circular channel based models; hence the circular channel methods are probably not reliable to use directly for non-circular channels. This last conclusion is not that surprising since the most common flow pattern regime in microchannels is annular

flow, which is a film flow that will react to capillary forces to pull the annular film into corners (a process that has no relationship to the single-phase flow hydraulic diameter definition).

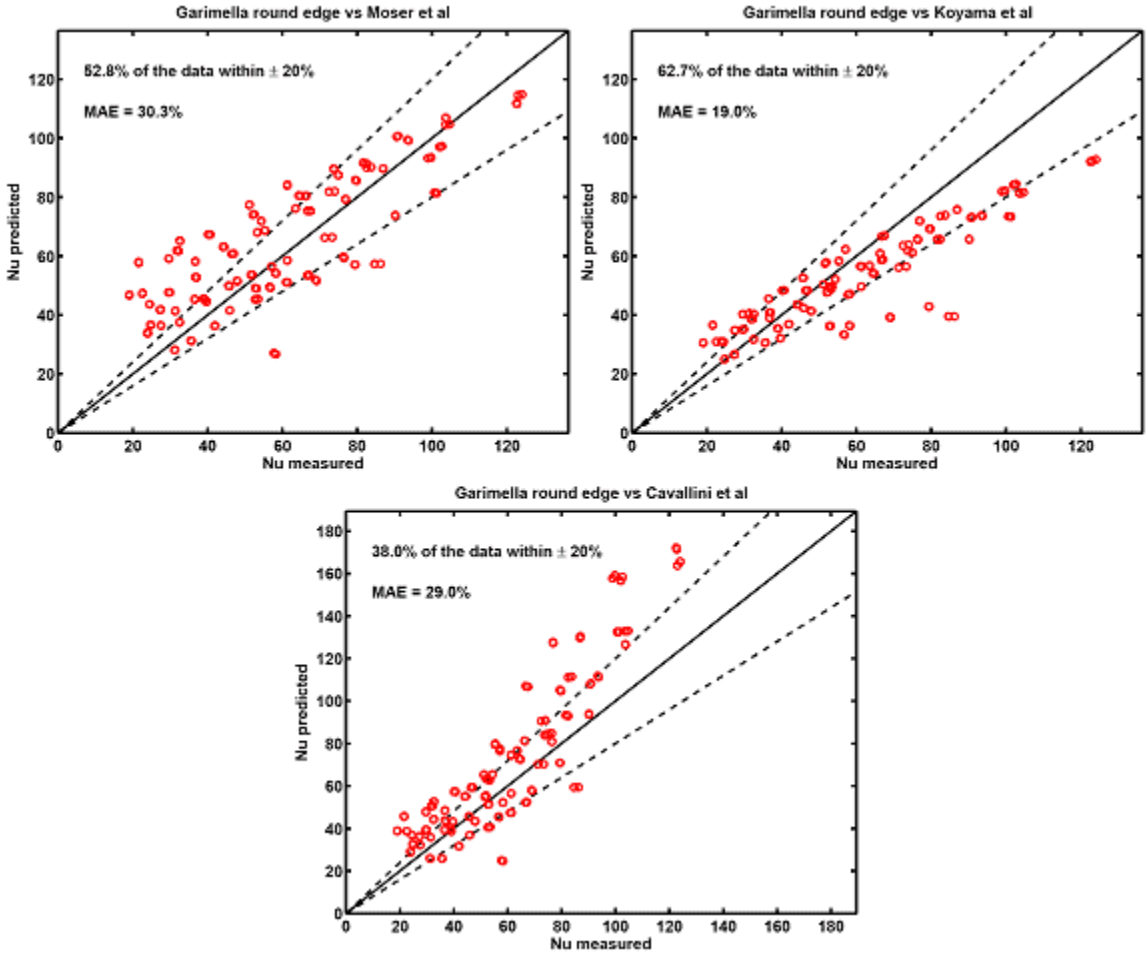

Figure 21.8. Predicted Nusselt numbers compared to the non-circular channel with round edge data of Agarwal, Bandhauer and Garimella (2007).

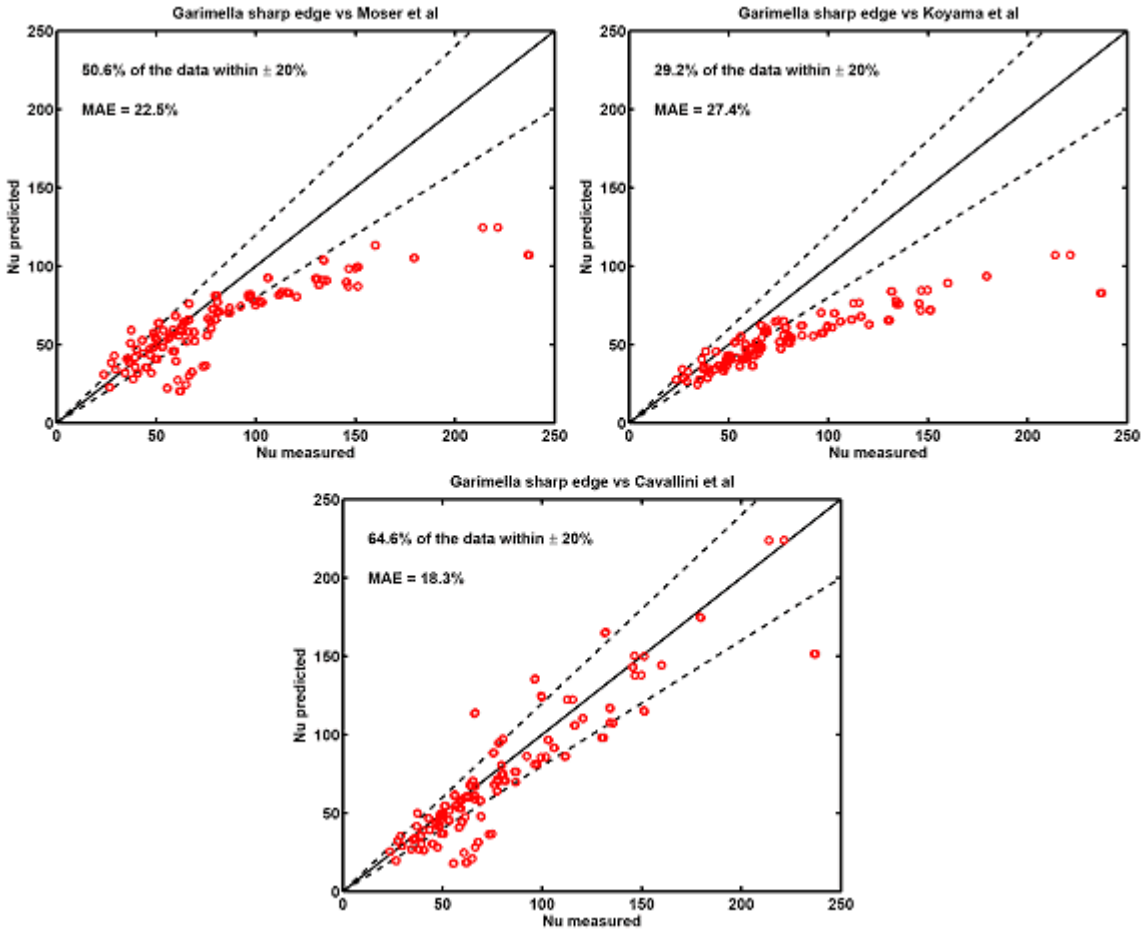

Figure 21.9. Predicted Nusselt numbers compared to the non-circular channel with sharp edge data of Agarwal, Bandhauer and Garimella (2007).

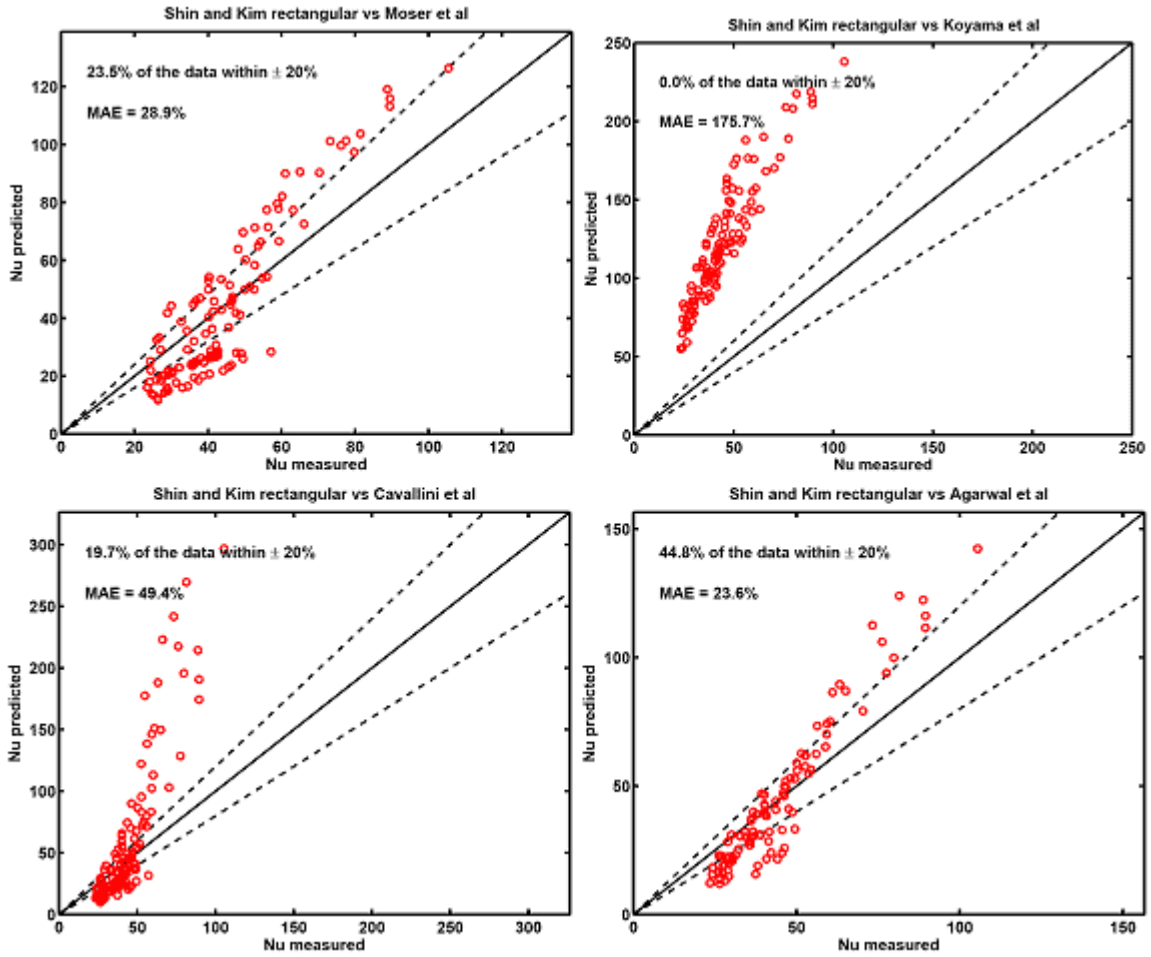

Figure 21.10. Predicted Nusselt numbers compared to the non-circular channel data from Shin and Kim (2004).

Reflecting further on the macroscale versus microscale aspect, existing macroscale condensation heat transfer methods do not often extrapolate well with respect to predicting very small channel or microchannel data in various published comparisons. With respect to this point, it is interesting to compare the above microscale methods to one another and to one of the leading macroscale methods, that of Thome, El Hajal and Cavallini (2003) described in Chapter 8. Extrapolating their flow pattern based method here to 1.0 and 3.0 mm channels (their method is valid down to 3.14 mm), one can assume that no stratified type of flow exists and hence one can utilize only their annular flow film condensation expression to such small channels, which is the dominant flow regime covering a wide range of vapor qualities in microchannels. Figure 21.11 depicts four such comparisons. As can be seen for several R-134a simulations at selected mass velocities and diameters, the macroscale annular flow model falls into the middle of the four microscale predictions. Furthermore, the predicted trends are all quite similar. Hence, the difference between macroscale and microchannel intube condensation seems to be less noticeable than one might expect, at least at these conditions, leaving the door open to the possible future development or confirmation of one method for the entire range of diameters. On the other hand, microscale condensation also has operating flow rates down into the laminar annular flow regime whilst most methods do not account for this transition in heat transfer mechanism across the film from turbulent mixing to pure conduction, either implicitly or explicitly. Hence, heat transfer predictions at low mass velocities with liquid film Reynolds numbers below ~1000-1500 may not be accurate using methods based mostly on turbulent annular film condensing data.

Finally, based on these *very* limited comparisons, the most consistent results can be expected to be obtained with the method based on test conditions most similar to the planned application. More work, both experimental and theoretical, is required to achieve a reliable, accurate general prediction method for circular and non-circular microchannels.

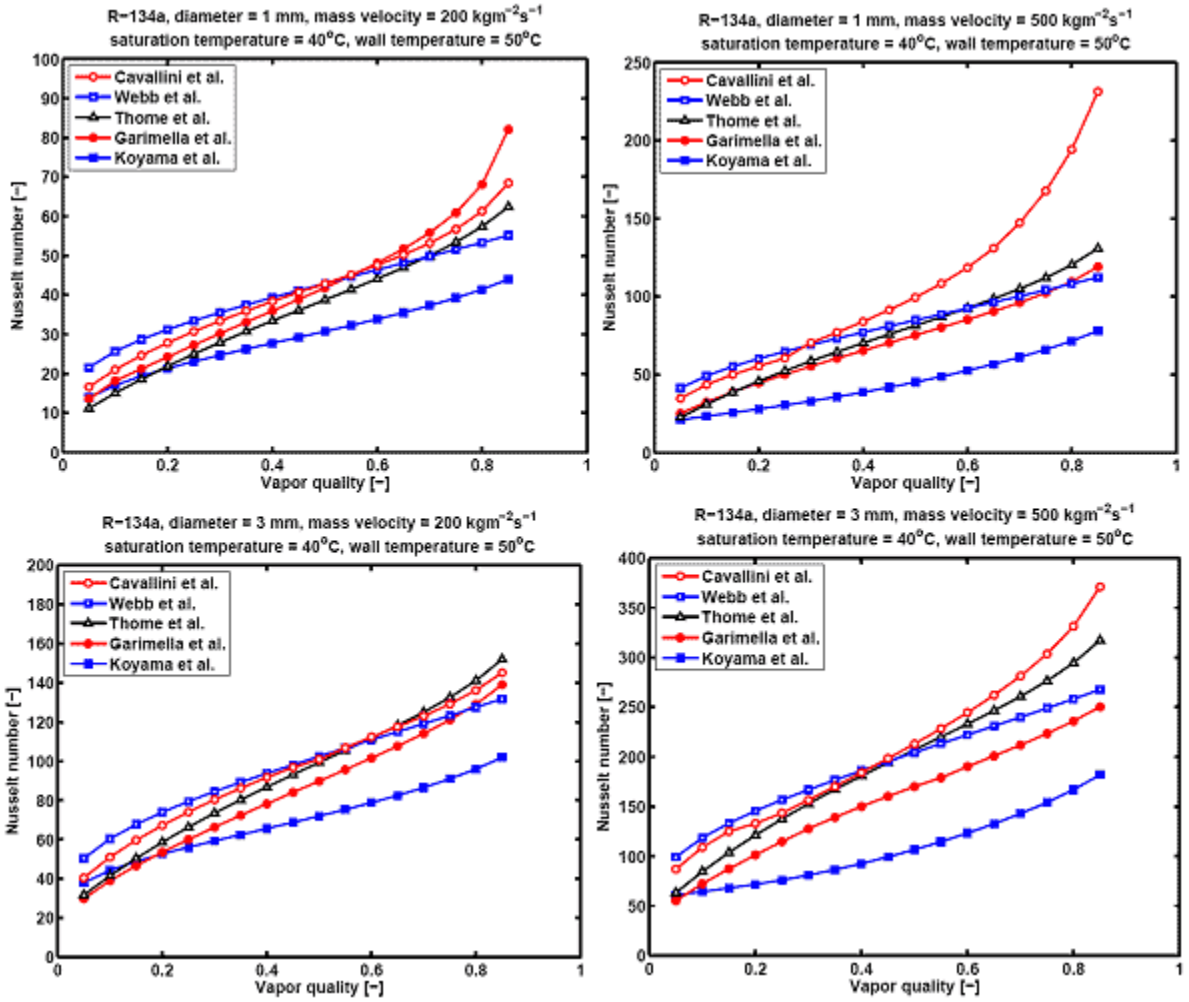

Figure 21.11. Comparison of prediction methods for R-134a in small channels.

21.5 Numerical Modeling of Condensation in Microchannels

Condensation in small channels has received increasing attention in recent years with particular emphasis on how to enhance heat transfer to enable even more compact heat exchangers. Recently, numerical modeling of the condensation process, in particular for *annular flows with laminar liquid films*, has gained a foothold in describing the process from a fundamental basis and providing predictions of local condensation heat transfer coefficients in circular and non-circular channels, with or without earth gravity, for horizontal, vertical or other orientations. A brief overview of this work is presented here. Since the details of numerical models and their implementation are quite complex, the interested reader is recommended to consult the original papers addressed in this summary. Please note that all of the following models cover so far only laminar condensate films (with or without interfacial vapor shear), but

not turbulent films. Empirical methods for implementing the effect of interfacial shear on film condensation have been presented in Chapter 7 for those interested.

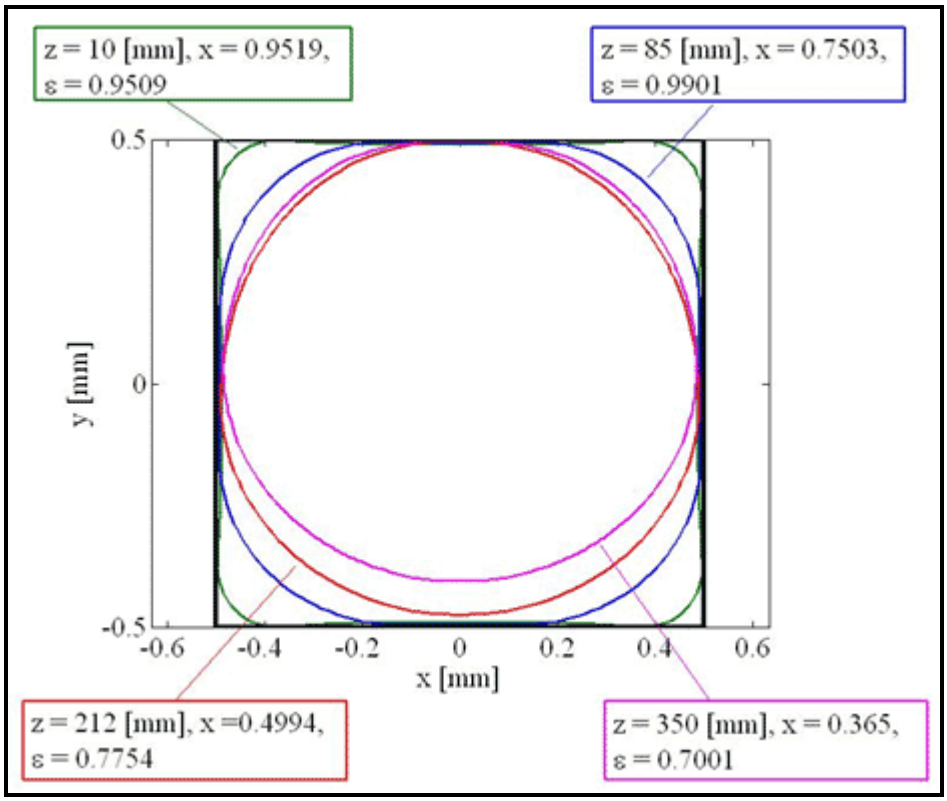

Figure 21.12. Condensate profile predicted by the Wang and Rose (2005, 2006) model.

Wang and Rose (2005, 2006) proposed the first detailed theoretical model to predict film condensation heat transfer of R134a, R22 and R410a vapor flowing inside horizontal circular, square, rectangular and equilateral triangular microchannels. Some of the assumptions used is developing their numerical model were: (a) the flow in the condensate film is laminar, (b) the wall temperature is uniform and constant, (c) the gravity is constant in magnitude and orientation, (d) the thermal inertia of the condensate is negligible, (e) the fluid properties are constant in space and time, (f) the momentum flux contributions are ignored in the momentum equations for simplification, and (g) the shear of the vapor phase core on the condensate is implemented using conventional single-phase friction factor relations. They then proceeded to model the liquid condensate to obtain its geometrical profile around the perimeter of various shaped channels. Then, using the calculated the local film thickness around the perimeter and assuming one-dimensional heat conduction, the perimeter-averaged heat transfer coefficient was obtained. Although this is a two-dimensional model (that is, it does not take into account all the axial terms), by simulating the flow at different local vapor qualities along the channel, the variation in the film profile due to the force balance and perimeter averaged heat transfer coefficient with respect to channel length (or vapor quality) was obtainable. Their work marked a very important advance in the understanding of microchannel condensation since it opens the door to simulating channel geometries for the particular fluid at the desired operating conditions, allowing one to find an optimum channel shape and size without having to expensively test numerous possibilities. The most important mechanism that enhances the heat transfer in non-circular channels during condensation is the thinning of the condensate film as it is pulled towards the corners, a flow generated by the pressure gradient induced by the surface tension forces (capillary forces) in the corners. Figure 21.12 depicts an example of such a cross-sectional view of the condensate for R134a at predicted by the Wang and Rose (2005, 2006) model for a saturation temperature of 50°C,

uniform wall temperature of 44°C and mass velocity of 300 kg/m^{2}s in a square horizontal channel of 1.0 mm by 1.0 mm at normal earth gravity. The liquid film profiles are shown at various void fractions (ε), vapor qualities (x), and distances from the entrance (z), clearly illustrating the effects of gravity and surface tension.

A condensation model based on the lubrication theory for predicting water condensation on curvilinear fins has been proposed by Kabov, Marchuk and Radionova (2007), showing the importance of the capillary forces and the effect on the film thickness distribution on the surface of contoured fins. Their model in fact is for *external* condensation, but one can imagine its application also to internal flows with negligible vapor shear. This model showed the effectiveness of optimizing the contour to achieve condensate drainage from the fin tip to the base to obtain very high heat transfer coefficients over a large portion of the fin's surface.

For internal condensing flows in microchannels at *very small* flow mass velocities, i.e. for mass velocities of about 15 kg/m^{2}s or less, Miscevic at al. (2007) proposed a one-dimensional numerical model for capillary condensation in circular microchannels. Some videos of this process taken by his team can be found in Chapter 1 of this book. They focused in particular on the effects of the instabilities occurring at very low mass fluxes induced by surface tension forces that are very important in capillary driven flow loops. Miscevic, Lavieille and Piaud (2009) have further advanced their model for condensation of pure fluids in the capillary flow regime.

More recently, Wu at al. (2009) presented a three-dimensional numerical model for steady-state annular condensation in rectangular microchannels with a constant heat flux boundary condition (this neglects the thermal wall heat conduction created by the variation in the local heat transfer coefficient around the perimeter and length of the channel). Hence, they have worked on a uniform heat flux boundary condition while Wang and Rose (2005, 2006) worked on a uniform wall temperature boundary condition. To simplify the problem and reduce computational time, their model divided the condensate flow field into two: a thin-film region on the faces and a meniscus region in the corners. They then showed that the average heat transfer coefficient in the thin film is much larger than that occurring in the meniscus region and concentrated their numerical calculations on the thin film region.

Nebuloni and Thome (2007, 2010a) have presented both two-dimensional and three-dimensional numerical models for condensation of annular flow with laminar liquid films for circular and non-circular channels. In particular, their method is based on a curvilinear coordinate system and was implemented including the following effects:

- the surface tension source term is calculated based on the three-dimensional curvature of liquid-vapor interface;
- the axial shear stresses due to the relative velocity difference of vapor and liquid phases are included (using conventional single-phase friction factor methods);
- a time dependent three-dimensional gravity field is included (their model covers normal gravity, microgravity, transient magnitude or gravity and a changing orientation of gravity with time);
- unsteady contributions in the momentum and mass conservation equations and momentum flux contributions are included, not excluded, in the model;
- interfacial resistance, disjoining pressure and liquid-vapor mass transfer are implemented, thus allowing the model to be scaled down to ultra micro-channel sizes (< 50 μm);
- conjugate heat transfer effects.

Regarding the last point, besides the conventional boundary conditions of: (*i*) an imposed heat flux (uniform in time and space) and (*ii*) an imposed uniform and constant wall temperature, in Nebuloni and

Thome (2010b) they added conjugate heat transfer effects of the wall and cooling fluid into the energy equation in their numerical model also for: (iii) an imposed heat flux (variable in time and space) and (*iv*) a single-phase convective cooling boundary condition encountered in numerous practical applications and experimental test setups. For instance, this means that if an imposed heat flux boundary condition is assumed, the wall thermal conduction into axial and peripheral directions is taken into account. The model has also been compared with the results presented by Wang and Rose (2005, 2006), showing a good agreement when the new implemented features in the Nebuloni-Thome model are suppressed. Furthermore, three sets of experimental data from widely quoted experimental studies on small diameter channels were analyzed and compared to the predicted values of the numerical model, showing a good agreement with an average error of 11%, very close to the typical experimental error range for this type of measurement in small channels, with nearly all of the data predicted within ±20%. Their model is of particular interest to applications in the aerospace, avionics, automotive, naval, heat pipe, etc. industries for systems utilizing ever smaller heat transfer channels with different shapes in situations with steady or transient gravity effects or transient variation of the flow channel with respect to gravity. The model is also a valuable tool, for example, for investigating the effects of micro-manufacturing tolerances on thermal performance.

Figure 21.13 shows the simulation of Nebuloni and Thome (2010a) at the same uniform wall temperature conditions simulated by Wang and Rose (2005, 2006) above. This graph shows the local heat transfer coefficient around the perimeter and along the length, illustrating the high heat transfer coefficients near the entrance and the variation around the perimeter and along the length of the channel.

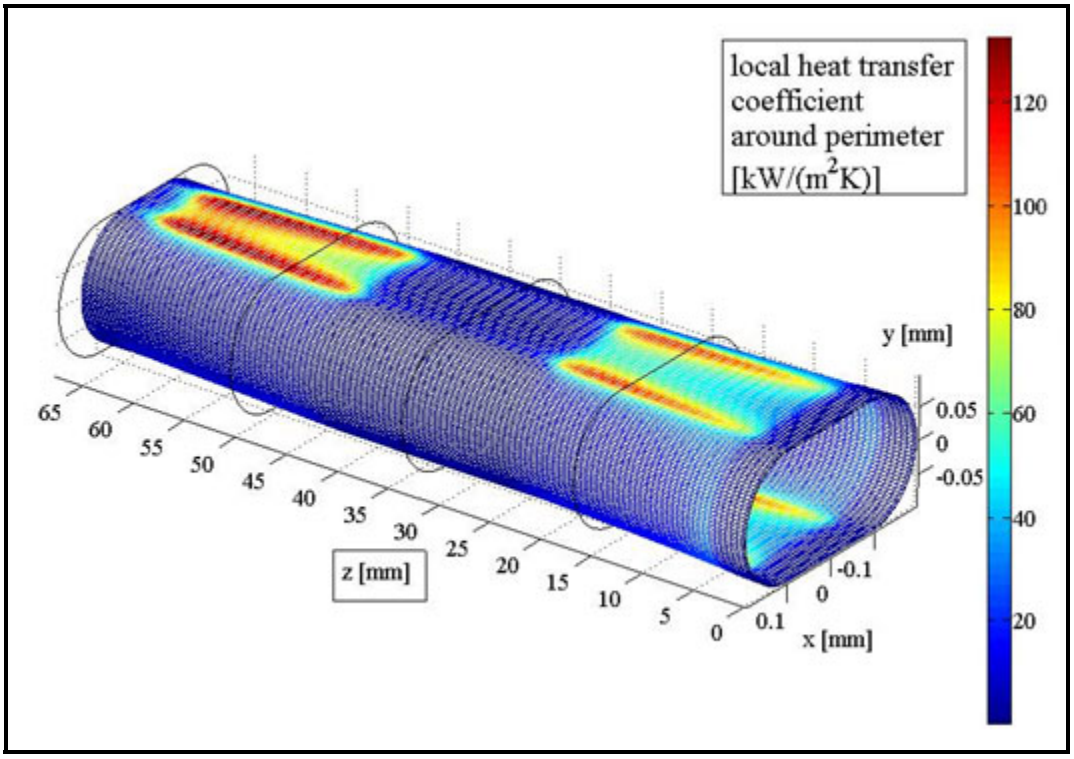

Figure 21.13. Condensation simulation of Nebuloni and Thome (2009, 2010) for R-134a at a saturation temperature of 50°C, uniform wall temperature of 44°C and mass velocity of 300 kg/m^{2}s in a square horizontal channel of 1.0 mm by 1.0 mm.

Nebuloni and Thome (2010b) and Nebuloni, Del Col and Thome (2010) have simulated various "conjugate heat transfer" problems with wall conduction and convection boundary conditions, including

additional comparisons to experimental data. Figure 21.14 shows another simulation for a saturation temperature of 40°C, a nominally uniform wall heat flux of 25 kW/m^2 and a mass velocity of 300 kg/m^{2}s in a flattened horizontal channel at normal earth gravity. The vapor quality variation from inlet to outlet is 0.511 while the hydraulic diameter is 0.270 mm. The heat conduction in the wall (assumed to be stainless steel that is 1.0 mm thick with a thermal conductivity of 16.5 W/mK) has been modeled by the "conjugate heat transfer" version of their model. In this case, the heat flux is uniform around the perimeter of the channel but not along the axis of the channel. While the heat flux remains within 10% of the mean value near the entrance, exit and midpoint of the channel, it goes through two peaks that are about 1.6 times that of the nominal value, illustrating the significant effects that the axial conduction can have on microscale condensation heat transfer but which is usually neglected.

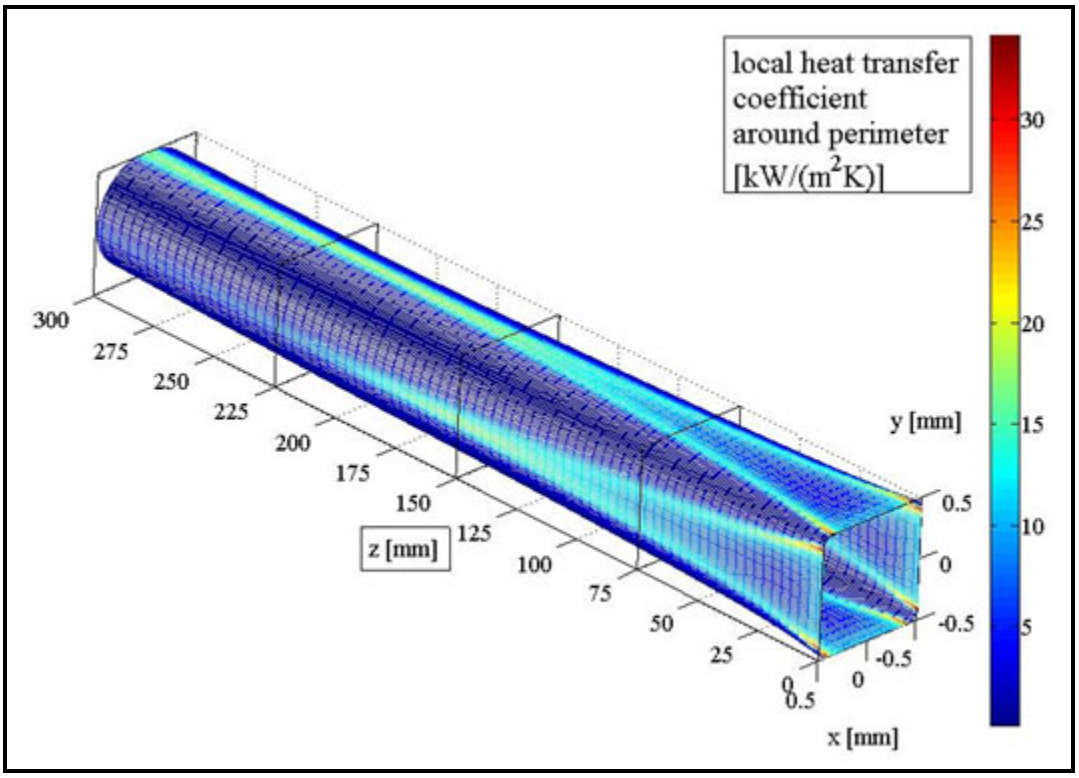

Figure 21.14. Condensation simulation of Nebuloni and Thome (2010b) for R-134a at a saturation temperature of 40°C in a flattened channel illustrating conjugate heat transfer effects from heat conduction in the wall.